Trans. of the Society of Instrument and Control Engineers
Vol.E-4, No.1, 68/78 (2005)

Time-period Analysis for Pulse Train Deinterleaving

Ken'ichi NISHIGUCHI*

This paper presents a new method for signal separation of interleaved pulse trains consisting of several pulse trains emitted from independent signal sources, some of which may only exist for a short time. The separation is based on the differences in the pulse repetition intervals (PRIs) of the signal sources. To detect each pulse train, we derive a map from the input signal to a function of two variables: time and PRI, which we call the PRI map. By taking the absolute value of the PRI map, we obtain a short-time PRI spectrum from which we can use thresholding to estimate the number of signal sources, their time duration, and the PRIs. The PRI map is an extension of PRI transform, which we previously proposed. The extension is based on time-period analysis. The construction of the PRI map resembles a wavelet transform. The difference is that a PRI map is a nonlinear transform, while the wavelet transform is linear. Simulation results are presented on the performance of the signal separation of interleaved pulse trains using the PRI map. Finally, performance analysis shows the detection ability of the PRI map for short pulse trains.

Key Words: signal separation, deinterleaving, pulse train, pulse repetition interval, time-period analysis

1. Introduction

The problem of signal separation for periodic pulse trains is called deinterleaving and arises in such fields as radar signal detection and computer communications [1)~8)]. In these fields, a receiver observes an interleaved pulse train, which is a composite signal comprised of many unknown sources with different pulse repetition intervals (PRIs).

As described in Wiley [1)], who reviews the conventional approaches to radar pulse deinterleaving, the deinterleaving of radar pulse trains is mainly based on the difference of pulse repetition intervals (PRIs).

If signals from all sources are sinusoidal, they can be easily separated by spectral analysis. More specifically, the number of signals and their frequencies are estimated from the number and locations of the peaks in the power spectrum. However, when signals are pulse trains, the power spectrum and the autocorrelation function again become periodical pulse trains; therefore, pulse train deinterleaving is a non-straightforward task.

To solve this problem, we previously proposed a method called PRI transform [7)], which is a nonlinear integral transform. PRI transform retains the peaks corresponding to PRIs and completely suppresses the peaks of the subharmonics in the autocorrelation function. Although the original PRI transform was vulnerable to timing jitter (PRI jitter), this was resolved by modifying the PRI transform [8)]. PRI transform allows us to obtain a kind of spectrum, referred to as PRI spectrum, from which we can estimate the number of signal sources and their PRIs.

However, to apply the PRI transform a constraint exists: each pulse train must contain enough pulses in the observation period. From a practical viewpoint, robustness to PRI jitters and being able to detect short pulse trains is desirable. In this paper, we satisfy these requirements by proposing a method called the PRI map, which is an extension of PRI transform by a time-period analysis. Though the former is also a nonlinear integral transformation like the latter, it has a feature that leads to a time-varying PRI spectrum using moving windows whose width is proportional to PRIs. By this extension, we show that pulse trains become detectable even if their PRIs are jittered, and they exist for short time periods in the observation period.

The organization of this paper is as follows. In Section 2, we formulate the problem and show the limitations of deinterleaving by PRI transform. In Section 3, we describe a deinterleaving method by PRI map proposed in this paper and simulation results. In Section 4, we analyze the performance of the PRI map. Finally, Section 5 draws some conclusions.

2. Formulation of the problem

Let $t_n,\ n = 1, 2, \cdots, N$ be the times of arrival (TOAs) of pulses. If we consider TOA the only parameter of each pulse, the pulse train can be modeled as a sum of unit impulses,

* Advanced Technology R&D Center, Mitsubishi Electric Corporation, Amagasaki (then)
Frontier Research Center, Osaka University, Suita (now)

$$g(t) = \sum_{n=1}^{N} \delta(t - t_n), \tag{1}$$

where $\delta(\cdot)$ is the Dirac delta function. Though an actual pulse has finite width and amplitude, we represent it by an impulse because only its TOA is used as a parameter.

We assume that the pulse train contains signals from several sources with different PRIs. In this case the pulse train can be represented as

$$g(t) = \sum_{\mu=1}^{M} g_\mu(t), \tag{2}$$

$$g_\mu(t) = \sum_{n=1}^{N_\mu} \delta(t - (n + \eta_\mu)p_\mu), \tag{3}$$

where M is the number of signal sources, N_μ is the number of pulses contained in source μ, and p_μ and η_μ are its PRI and phase, respectively.

The deinterleaving problem treated here is to estimate the number of signal sources M and their PRIs $p_\mu, \mu = 1, \cdots, M$. Equation (3) represents an ideal case in which the PRIs are fixed and there are no missing pulses. In actual situations, however, PRIs may be jittered, and pulses may be missing. Moreover, we must treat cases in which the number of pulses N_μ is small.

The PRI transform of signal $g(t)$ is defined by [7)]

$$D(\tau) = \int_{-\infty}^{\infty} g(t)g(t + \tau)e^{2\pi i t/\tau} dt, \tag{4}$$

where τ is the PRI variable ($\tau > 0$). If the input signal is a pulse train of the form of (1), its PRI transform contains an integral of the product of two δ functions. This integral is a convolutional type, and the convolution of two δ functions is strictly defined by Schwartz's distribution [9)] in the following formula:

$$\int_{-\infty}^{\infty} \delta(s - t)\delta(t) dt = \delta(s). \tag{5}$$

Using the above formula, the PRI transform of the pulse train of (1) is represented as

$$D(\tau) = \sum_{m=2}^{N} \sum_{n=1}^{m-1} \delta(\tau - (t_m - t_n))e^{2\pi i t_n/\tau}. \tag{6}$$

In particular, when the pulse train comes from a single signal source, i.e., $t_n = (n + \eta)p,\ n = 1, 2, \cdots, N$, it holds that

$$D(\tau) = (N - 1)\delta(\tau - p)\exp(2\pi i\eta) + \sum_{l=2}^{N-1} \delta(\tau - lp)\frac{\sin(N\pi/l)}{\sin(\pi/l)} e^{\pi i(N+1+2\eta)/l}. \tag{7}$$

The first term on the right-hand side (RHS) represents an impulse located at the PRI, and the modulus of the coefficient equals $N - 1$. On the other hand, the second term represents impulses located at the integer multiples of the PRI, i.e., subharmonics, and the moduli of the coefficients are evaluated by

$$\left|\frac{\sin(N\pi/l)}{\sin(\pi/l)}\right| \le \frac{1}{\sin(\pi/l)} \le \frac{l}{2}, \quad l = 2, 3, \cdots. \tag{8}$$

Note that RHS does not depend on N; hence, as N increases, the subharmonics are relatively suppressed.

Due to these features, the number of signal sources and their PRIs can be estimated by applying PRI transform and thresholding. However, this method has a limit from a practical viewpoint, because pulses from each source must exist during most parts of the observation time. **Figure 1**a shows an example of an interleaved pulse train that contains some short signal sources (sources #1, #2, #4, and #5). The PRI transform of this input pulse train is shown in Fig. 1b. Clearly, detecting all the signal sources from Fig. 1b is difficult.

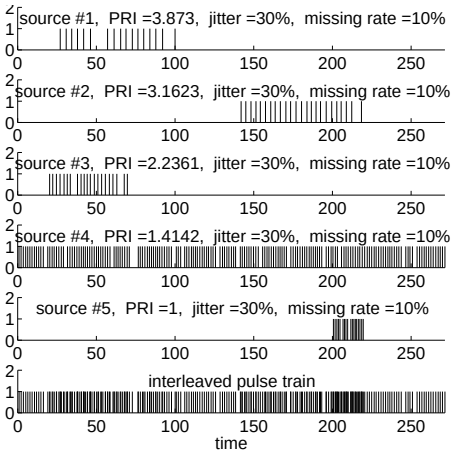

(a) Input pulse train

When there are multiple signal sources, the subharmonics for each source are suppressed in a similar manner.

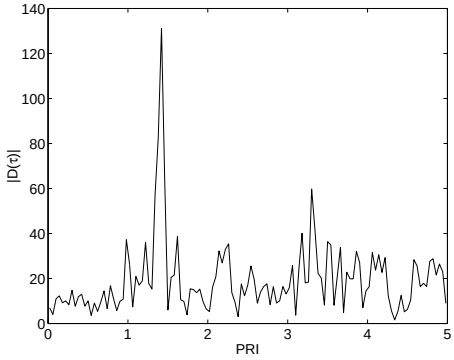

(b) PRI spectrum by modified PRI transform

Fig. 1 Modified PRI transform for a pulse train with short elements

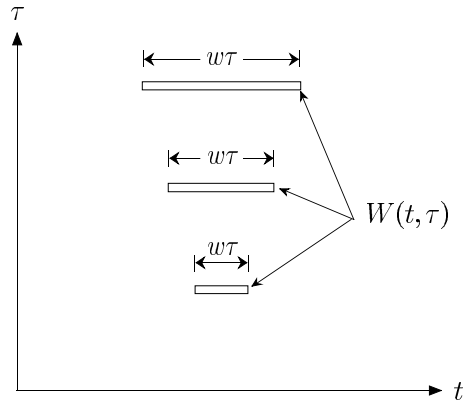

Fig. 2 Moving window for PRI map

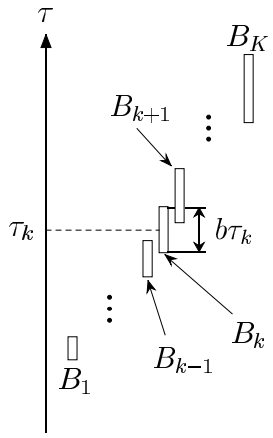

Fig. 3 Overlapped PRI bins

3. Time-period analysis of pulse trains

3.1 PRI map

The limitation of PRI transform described in the preceding section is common to the Fourier transform used to detect localized signals in general signal processing problems. The limitation of the Fourier transform is effectively overcome by time-frequency analysis using wavelet transforms [10),11)]. From the same viewpoint, we propose time-period analysis for pulse train deinterleaving.

For input signal $g(\cdot)$, we define the PRI map as

$$D(t,\tau)=\int_{s\in W(t,\tau)} g(s)g(s+\tau)e^{2\pi is/\tau}ds, \qquad (9)$$

where $W(t,\tau)=[t-\nu\tau/2, t+\nu\tau/2]$ is a moving window (see **Fig. 2**) and $\nu>0$ is a constant. The integrand is identical to the PRI transform and the difference is the integration range: the PRI map is the calculation of the PRI transform only in the moving windows. The center of the window is located at time t. The width of the window is $\nu\tau$, which is set to be proportional to PRI τ for the same reason as the wavelet transform. For example, if $w=10$, PRI transform is calculated in the interval with width corresponding to 10 pulses for each τ. Thus, the PRI map is a wavelet-like extension of PRI transform that maps input signal $g(\cdot)$ to a function of time t and PRI τ.

When $g(t)$ is a pulse train described by (1), the PRI map becomes

$$\begin{aligned} D(t,\tau)&=\sum_{m=2}^{N}\sum_{n=1}^{m-1}\int_{s\in W(t,\tau)}\delta(s-t_n)\\ &\qquad\times\delta(s+\tau-t_m)e^{2\pi is/\tau}ds\\ &=\sum_{m=2}^{N}\sum_{n=1}^{m-1}\delta(\tau-(t_m-t_n))e^{2\pi it_n/\tau}I_{W(t,\tau)}(t_n), \end{aligned} \qquad (10)$$

where $I_{W(t,\tau)}$ is the defining function of set $W(t,\tau)$. For numerical calculation, the PRI map must be a discrete form. For this reason, we divide the τ-axis into small intervals referred to as PRI bins (see **Fig. 3**). We denote the distance between the centers of adjacent PRI bins by $\Delta\tau$ and let

$$\tau_k=(k-1/2)\Delta\tau, \quad k=1,\cdots,K \qquad (11)$$

be the centers of the PRI bins. Here K, which denotes the number of PRI bins, is selected so that $K\Delta\tau$ exceeds the upper limit of PRI to be searched for. We represent the PRI bins by

$$B_k=[(1-b/2)\tau_k,(1+b/2)\tau_k], \quad k=1,\cdots,K, \qquad (12)$$

where $b>0$ is a constant. Then the widths of the PRI bins are $b\tau_k, k=1,\cdots,K$, and they overlap their neighborhood bins. The overlap considers the PRI jitters of the pulse trains to be detected [8)]. Under these preparations, we define a discrete PRI map for a pulse train of (1) by

$$D_k(t)=\sum_{\{(n,m);t_m-t_n\in B_k,t_n\in W_k(t)\}} e^{2\pi it_n/\tau_k}, \qquad (13)$$

where $W_k(t)=W(t,\tau_k)$. Moreover, using $|D_k(t)|$, we define the PRI spectrum as a function of time. Since it corresponds to a time-varying spectrum in the time-frequency analysis, it can be called a time-varying PRI spectrum.

In the previously proposed modified PRI transform [8)], we introduced the shift of time origins along with the overlapped PRI bins and defined a discrete algorithm by

$$D_k=\sum_{\{(n,m);t_m-t_n\in B_k\}} e^{2\pi it'_n/\tau_k}, \qquad (14)$$

where t'_n is the changed value of t_n by the shift of the time origin. Due to this shift operation, the enlargement of the fluctuations of phase $2\pi t_n/\tau_k$ with time is suppressed. This is effective for long pulse trains. However, since the

PRI map is a PRI transform within moving windows, the enlargement of phase fluctuation is not significant, so in the PRI map we do not utilize the shift of time origins.

3. 2 Signal detection method from PRI map

If the PRI of a signal source is τ_k and its pulse train exists in moving window $W_k(t)$, then since the value of the PRI map of (13) is the sum of complex numbers with the same phase, it constructs a peak in the time-varying PRI spectrum. The subharmonics, which are located at the integer multiples of the PRI, are suppressed by the same principle as the PRI transform.

We detect pulse trains by thresholding the time-varying PRI spectrum. More specifically, if $|D_k(t)|$ exceeds a certain threshold, we determine that a pulse train with a PRI of τ_k exists at time t.

The detection threshold must be determined from the noise statistics. We describe it with a noise model in the following two sections.

3. 3 Noise model and false alarm probability

In the PRI map defined by (13), even if there is no pulse train whose PRI corresponds to PRI bin B_k, pulse pair (t_n, t_m) may exist that satisfies $t_m - t_n \in B_k$ and $t_n \in W_k(t)$. Then a complex number with modulus one is added to the PRI map. This is caused by the mutual interference of signal sources with different PRIs. Since such complex numbers in general have different phases, they are not accumulated; however, they constitute noise components of the PRI map and cause false alarms. Here, we analyze the false alarm probability with a Poisson arrival model first introduced in a previous paper [8].

We arbitrarily fix PRI bin B_k and moving window $W_k(t)$ and assume that the value of the PRI map is only generated by noise components, which means that no pulse train whose PRI corresponds to the PRI bin is contained in the moving window. We also assume that pulses are distributed uniformly in the moving window. Let ρ be the pulse density in the moving window. Although the pulses are actually elements of some pulse trains, the assumption of uniform distribution gives good approximation for the evaluation of the noise component of the PRI transform [8]. Since the PRI map is the PRI transform in the moving windows, we use the same assumption.

Let L be the number of pulse pairs whose left element is in the moving window and whose time difference is in the PRI bins. Since the width of the moving window is $w\tau_k$, there are an average of $\rho w\tau_k$ pulses in the window. In addition, since the width of the PRI bin is $b\tau_k$, for a fixed pulse the average number of pulses, whose time differences with the fixed pulse is in the PRI bin, is $\rho b\tau_k$.

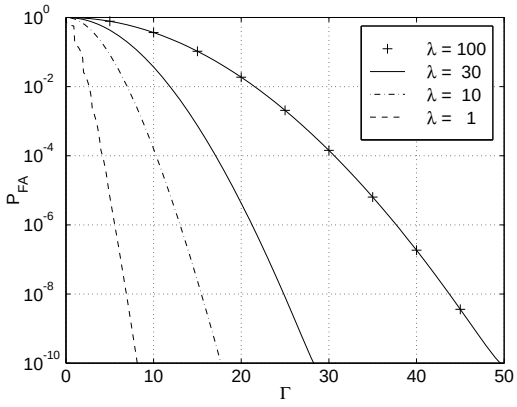

Fig. 4 False alarm probability of PRI map

The expectation of L, denoted by λ, is the product of the above quantities, i.e.,

$$\lambda = (\rho\tau_k)^2 bw. \tag{15}$$

Assuming that L pulses follow a Poisson distribution with parameter λ, the noise component of the PRI map is modeled by

$$D_{\mathrm{N}} = \sum_{j=1}^{L} e^{i\Theta_j}, \tag{16}$$

where $\Theta_j, j = 1, 2, \cdots, L$ are the independent random variables uniformly distributed in $[0, 2\pi]$. We define the noise intensity by

$$I_{\mathrm{N}} = \sqrt{E|D_{\mathrm{N}}|^2}, \tag{17}$$

which is calculated for the model of (16) as

$$I_{\mathrm{N}}^2 = E\sum_{\ell,j=1}^{L} E[e^{i(\Theta_\ell - \Theta_j)}|L] = EL = \lambda, \tag{18}$$

where E denotes expectation. Furthermore, the false alarm probability for threshold Γ is obtained as follows:

$$\begin{aligned} P_{\mathrm{FA}} &\equiv \mathcal{P}(|D_{\mathrm{N}}| \geq \Gamma) \\ &= 1 - \Gamma\int_0^\infty \exp[\lambda(J_0(s) - 1)]J_1(\Gamma s)ds, \end{aligned} \tag{19}$$

where $J_0(\cdot)$ and $J_1(\cdot)$ are the Bessel functions of orders 0 and 1, respectively. The derivation of (19) is shown in Appendix A. In **Fig. 4**, false alarm probabilities calculated by (19) are shown.

3. 4 Threshold determination from data

In applications, detecting signals at a given false alarm probability is desirable. For this reason, we numerically solve (19) with respect to Γ and set

$$\Gamma = h(\lambda; P_{\mathrm{FA}}). \tag{20}$$

In **Fig. 5**, the thresholds are plotted for each false alarm

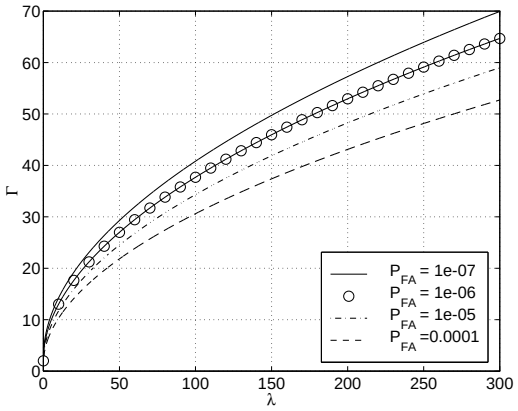

Fig. 5 Threshold of PRI map

probability as a function of λ. Although λ is a function of pulse density, the actual pulse density of a pulse train changes based on time. So when the number of pulses in moving window $W_k(t)$ is $N_k(t)$, we estimate the pulse density for each moving window by

$$\rho = \frac{N_k(t)}{w\tau_k}, \tag{21}$$

and λ by

$$\lambda = \frac{N_k^2(t)b}{w}, \tag{22}$$

and substituting that into (20) yields

$$\Gamma_k(t) = h(\frac{N_k^2(t)b}{w}; P_{\rm FA}). \tag{23}$$

We use this quantity as a threshold. It is an adaptive threshold that includes the measurement values of the data.

3. 5 Subharmonics

The subharmonics level of the PRI map can be evaluated by (8) as in the case of the PRI transform. We compare this level with the noise threshold. If we approximate the distribution of $D_{\rm N}$ of (16) by a two-dimensional normal distribution, the distribution of its modulus $|D_{\rm N}|$ is approximated by the Rayleigh distribution, and its probability density function is written as

$$f(r) = \frac{2r}{\lambda} e^{-r^2/\lambda}, \tag{24}$$

which becomes a good approximation when λ is large due to the central limit theorem. Then the false alarm probability can be approximated by

$$P_{\rm FA} \sim \int_{\Gamma}^{\infty} f(r)dr = e^{-\Gamma^2/\lambda}, \tag{25}$$

and solving that with respect to Γ and substituting (15) yields

$$\Gamma \sim (-\log P_{\rm FA})\sqrt{bw}\rho\tau. \tag{26}$$

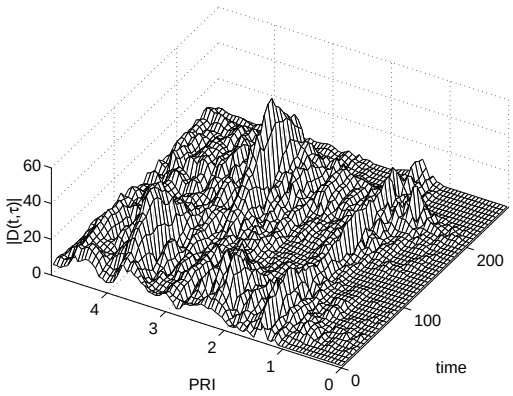

(a) Time-PRI spectrum by PRI map

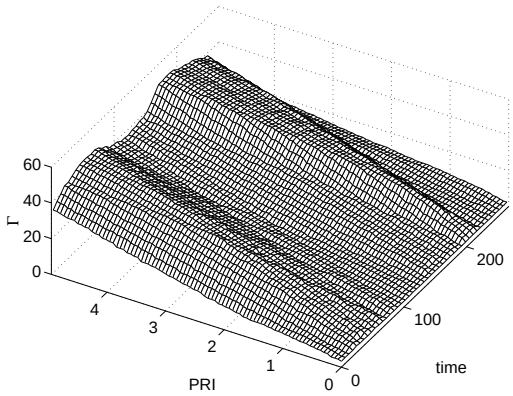

(b) Adaptive threshold for time-PRI spectrum

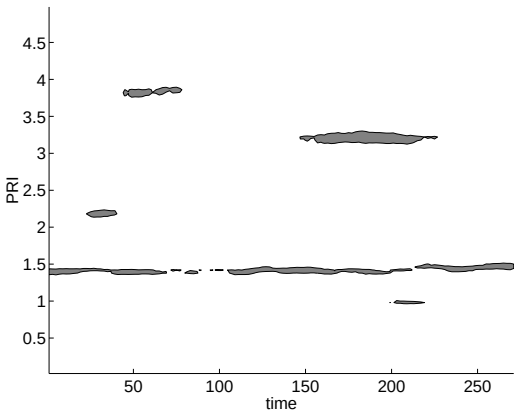

(c) Detected signals by PRI map

Fig. 6 Simulation result

We consider a pulse train with a PRI of p. Since the pulse density is $\rho = 1/p$, the threshold at the subharmonics of $\tau = lp$ becomes

$$\Gamma \sim (-\log P_{\rm FA})\sqrt{bw}l. \tag{27}$$

For example, if $P_{\rm FA} = 10^{-6}$, $b = 0.3$ and $w = 20$, then $\Gamma \sim 9.1l$, which is much larger than $l/2$ on the RHS of (8). Consequently, subharmonics levels are negligible compared with the noise threshold.

3. 6 Numerical example

In **Fig. 6**, we show a numerical example of pulse train

detection using the PRI map. The input pulse data are identical as the example of Section 2, which contains five signal sources, four of which are short pulse trains. For these input data, the time-varying PRI spectrum and the adaptive threshold of (23) are shown in Figs. 6a and b, respectively. Here, we set the parameters of the PRI map as $b = 0.3$ and $w = 20$. Also, we set the false alarm probability that determines the threshold as $P_{\rm FA} = 10^{-6}$. The region where the time-varying PRI spectrum exceeds the threshold is shown in Fig. 6c, which gives the detection result. As is apparent from this figure, by the PRI map method, the pulse train from each signal source is clearly detectable even if its PRI is jittered, if it is sporadic, or if some pulses are missing. Note, however, that the detected intervals are a little narrower than the actual intervals. This reflects that the number of pulses in the window is reduced at both ends of a pulse train, so detection ability is slightly degraded there.

4. Performance analysis

4. 1 Assumptions and conditions of detectability

The PRI map's detection performance is affected by its design parameters and the characteristics of pulse trains. The design parameters are b, the relative width of the PRI bins, and w, the relative width of the moving windows. To characterize the pulse trains, we fix a pulse train from a signal source to be detected and regard other pulses as mixing pulses. We define the following three parameters:

- ν : length of pulse train to be detected (number of pulses)
- ζ : PRI jitter width of pulse train to be detected
- q : average number of mixing pulses in a period of pulse train to be detected

Note that when the average PRI is τ and the PRI jitter width is ζ, PRIs are jittered in interval $[(1-\zeta/2)\tau, (1+\zeta/2)\tau]$, where we assume that the distribution is uniform. We also assume that mixing pulses occur in Poisson arrival, as in Section 3. 2. We denote by ρ the pulse density of an input pulse train. Then the average number of mixing pulses is given by $q = \rho\tau - 1$. For the pulse train of Fig. 1a, q varies in the range of $0 \le q \le 5.5$, as shown in **Fig. 7**.

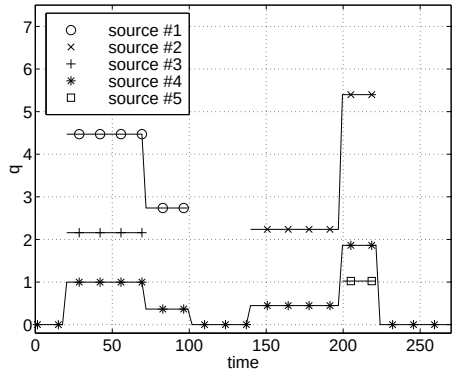

Fig. 7 Average number of mixing pulses per period for a case shown in Fig. 1a

Next, we specify the detectability condition for performance analysis. We fix a PRI bin and a moving window in which the pulse train to be detected is contained. Let $D_{\rm S}$ be the PRI map there. For the pulse train to be detectable, given threshold Γ, it must satisfy

$$|D_{\rm S}| \ge \Gamma. \tag{28}$$

Since it is complicated to obtain the distribution of $D_{\rm S}$, which is a random variable, we define the signal intensity by

$$I_{\rm S} = \sqrt{E|D_{\rm S}|^2}, \tag{29}$$

and specify the detectability condition as

$$I_{\rm S} \ge \Gamma. \tag{30}$$

To calculate Γ, we use (20), whose argument λ is obtained by (15). If we set $\nu' = \min(\nu, w)$, since the average number of pulses in the moving window is $qw + \nu'$, the pulse density is given by $\rho = (qw + \nu')/w\tau$, and we have

$$\lambda = \frac{(qw + \nu')^2 b}{w}. \tag{31}$$

In addition, the false alarm probability in (20) is set as $P_{\rm FA} = 10^{-6}$, which was also used in the numerical example.

4. 2 Signal intensity

Under the condition of the preceding section, we analytically obtain the signal intensity of the pulse train to be detected. By τ, we denote both the average PRI of the pulse train to be detected and the center of the PRI bin that contains the signal. Let $t_1, t_2, \cdots, t_\nu$ be the TOAs of the pulses in the pulse train to be detected, which satisfy the following relations by the assumption of the preceding section:

$$t_n = t_{n-1} + \tau(1 + X_{n-1}), \quad n = 2, 3, \cdots, \nu, \tag{32}$$

where $X_n, n = 1, 2, \cdots$ are random variables that represent the PRI jitter and they are mutually independent and distributed uniformly in $[-\zeta/2, \zeta/2]$.

When other pulses are mixed with the pulse train to be detected, the PRI map at the PRI bin where the signal exists can be approximated by

$$D_{\mathrm{S}} = \sum_{n=1}^{\nu}(1 + U_n + V_n)e^{2\pi i t_n/\tau} + D'_{\mathrm{N}}, \tag{33}$$

where U_n and V_n are the number of mixing pulses that constitute a pulse pair whose left and right elements are t_n, respectively. Also, D'_{N} is part of the PRI map that is attributed by pulse pairs whose both elements are mixing pulses.

Since the density of mixing pulses is q/τ and the width of the PRI bin is $b\tau$, the expectations of U_n and V_n are given by

$$EU_n = EV_n = bq. \tag{34}$$

If the mixing pulses are modeled by a Poisson model, the expectations of the square of the above variables become

$$EU_n^2 = EV_n^2 = bq + (bq)^2. \tag{35}$$

The expectation of the square of D'_{N} can be calculated in the same way as (15) and (18), and then we have

$$E|D'_{\mathrm{N}}|^2 = q^2 bw. \tag{36}$$

Using these relations, the signal intensity defined by (29) is written as

$$I_{\mathrm{S}}^2 = (1 + 2bq)^2 I_0^2 + (qw + 2\nu')bq, \tag{37}$$

where $\nu' = \min(\nu, w)$ and I_0 is the signal intensity in cases of no mixing pulses and is given by

$$I_0^2 = \nu' \frac{1 + \mathrm{sinc}(\zeta)}{1 - \mathrm{sinc}(\zeta)} - \frac{2\mathrm{sinc}(\zeta)[1 - \mathrm{sinc}^{\nu'}(\zeta)]}{[1 - \mathrm{sinc}(\zeta)]^2}. \tag{38}$$

The details of these signal intensity calculations are shown in Appendix B.

4. 3 Detection performance of PRI map

The merits of the PRI map lie in the detectable characteristics of pulse trains, even if they are so short that they are only included in part of the observation time and their PRIs are jittered. Questions remain: How short is the detectable pulse train? What size of PRI jitter width is allowable? We quantitatively evaluate these detection abilities using analytical representations derived in the preceding section.

(A) Minimum length of detectable pulse train

When the length of the pulse train to be detected is ν, then in general, a moving window with $w = \nu$ width gives the best result. This is because, if the moving window is wider than that, then the noise intensity increases while the signal intensity does not change, and conversely, if the moving window is narrower than that, then the degree of the reduction of the signal intensity is larger than the noise intensity. Therefore, we investigate the detection ability under the condition where $w = \nu$. As will be stated afterward, there are also cases where the noise intensity does not increase even if w increases, which happens when q is very small; however these cases are exceptional.

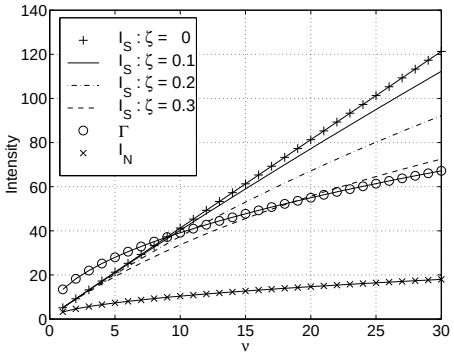

Fig. 8 Signal intensity and threshold, $b = 0.3$, $w = \nu$, $q = 5$

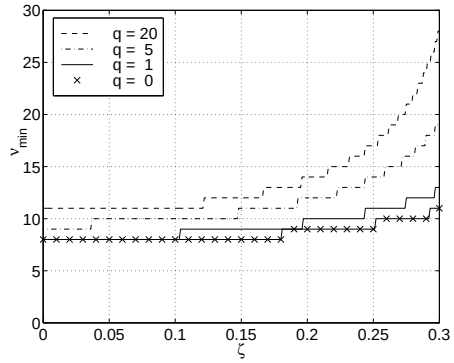

Fig. 9 Minimum length of pulse train, $b = 0.3$, $w = \nu$

In **Fig. 8**, signal intensity I_{S} calculated by (37), noise intensity I_{N} calculated by (18), and threshold Γ calculated by (20) are plotted as a function of ν. The values of the parameters are $b = 0.3$ and $q = 5$. As shown in this figure, when ν is small the threshold is larger than the signal intensity; as ν increases, the signal intensity grows faster than the threshold, and the signal becomes detectable at ν, denoted by ν^*_{min}. ν^*_{min} is a function of b, ζ, and q. In **Fig. 9**, ν^*_{min} is plotted as a function of ζ, where we set $b = 0.3$. From this figure, when PRI jitter is small ($\zeta \leq 0.15$), a short pulse train around 10 pulses is detectable, and even when ζ is larger than that, a pulse train of less than 20 pulses is detectable under the condition that $q \leq 5$ and $\zeta \leq 0.3$.

A pulse train with a length of ν^*_{min} is only detected in cases in which the window width is equal to it. Actually w must be determined previously; hence we must obtain the length of a pulse train that is detectable by a window with w width. We denote its minimum length by ν_{min}, which is a function of b, w, ζ, and q. In exceptional cases, the pulse train is undetectable even if ν is increased to w.

In this case $\nu_{\min}$ is indefinable. In **Fig. 10**, $\nu_{\min}$ is plotted with w fixed. From this figure, for example, if jitter width satisfies $\zeta \leq 0.15$ and the number of mixing pulses satisfies $q \leq 5$, then pulse trains with less than or equal to 10 pulses are detectable by the $w = 10$ window (see Fig. 10a). Also, if jitter width satisfies $\zeta \leq 0.3$ and the number of mixing pulses satisfies $q \leq 5$, then pulse trains with less than or equal to 20 pulses are detectable by the $w = 20$ window (see Fig. 10b). The latter case is close to the condition of the numerical example in the preceding section.

In general, if the width of a moving window increases, then $\nu_{\min}$ increases. Cases in which q is very small (in Fig. 10, only the case of $q = 0$ corresponds to it) are exceptional; if w increases, then $\nu_{\min}$ decreases. This reflects the fact that in this case the λ of (31) becomes a decreasing function of w and the threshold is decreasing.

Figure 10c shows a case in which the width of the moving window is very large ($w = 100$). In this case, the values of $\nu_{\min}$ are very large; for example, when $q = 5$ and $\zeta = 0.3$, it exceeds 60. The PRI transform can basically be regarded as a PRI map with very wide moving windows. In this case, however, the the length of the pulse train required for detection becomes too large (as seen above), and it is interpreted as a drawback of the PRI transform.

(B) Maximum jitter width of detectable pulse train

So far, we have analyzed the performance by fixing the width of the PRI bin to $b = 0.3$. Here, we vary b and analyze to what extent PRI jitter is allowable.

In **Fig. 11**, signal-to-threshold ratio I_S/Γ is plotted as a function of PRI jitter width ζ, where the values of the parameters are $b = 0.2$ and $w = \nu = 20$. If ratio I_S/Γ is larger than one, then a pulse train is detectable. In this calculation, when ζ is greater than b, we assume that signal intensity is reduced to b/ζ times of I_0, and instead of (37) we used

$$I_S^2 = [(1 + 2bq)(b/\zeta)I_0]^2 + (q^2 + 2q)b\nu. \qquad (39)$$

Fig. 11 shows that if we increase ζ, I_S/Γ gradually decreases and reaches one at some ζ, denoted by $\zeta_{\max}$. This $\zeta_{\max}$ is a function of b, w, ν, and q. In **Fig. 12**, $\zeta_{\max}$ is plotted as a function of b, where we set $w = \nu = 20$. From the figure, we find that since $\zeta_{\max} > b$ when $q \leq 5$, $\zeta \leq 0.3$, we can cope with PRI jitter by setting b to the possible maximum jitter width. We also find that by increasing b to 0.4, $\zeta_{\max}$ can be increased to about 0.35.

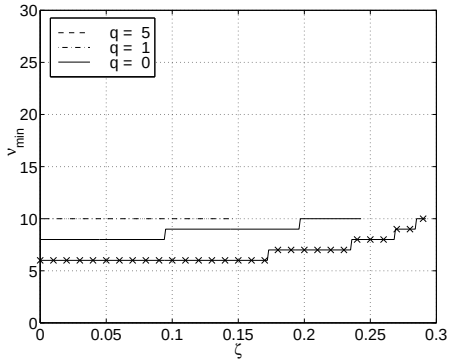

(a) $w = 10$

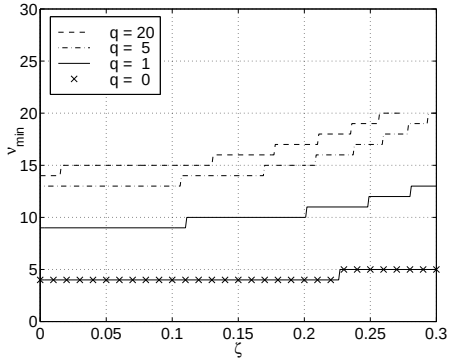

(b) $w = 20$

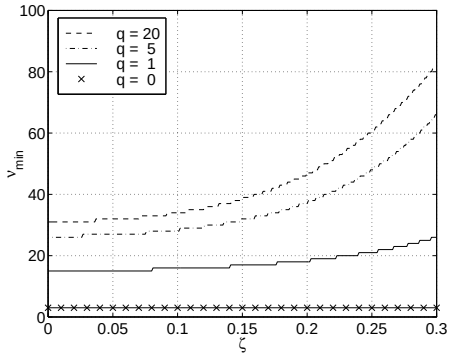

(c) $w = 100$

Fig. 10 Minimum length of pulse train when w is fixed: $b = 0.3$

On the contrary, from the viewpoint of resolution, smaller b is better, because the difference between PRIs must be greater than $b \times$ PRI to distinguish two pulse trains; the larger b is, the less resolution. Consequently, b must be determined in consideration for the above two conflicting requirements.

5. Conclusion

We proposed the PRI map method that enables detection of short pulse trains whose PRIs are possibly jittered. This method is an extension of PRI transform. The extension resembles that from Fourier transform to wavelet transform, and the PRI map obtained by the extension is a function of both time and PRI. Simulation and per-

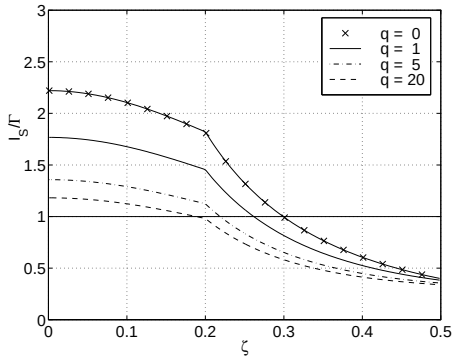

Fig. 11 Signal-to-threshold ratio: $b = 0.2$, $w = \nu = 20$

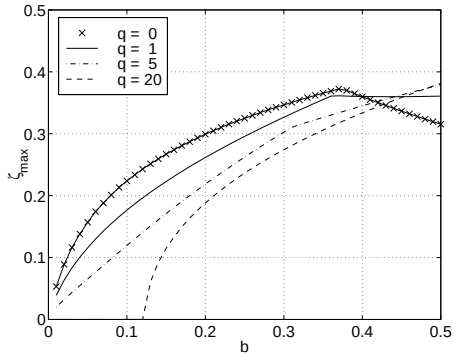

Fig. 12 Maximum width of PRI jitter: $w = \nu = 20$

formance analyses verified that it can detect short pulse trains with lengths from 10 to 20 pulses whose PRIs are possibly jittered. From these characteristics, the PRI map method is expected to be extensively applied to PRI analysis.

Acknowledgments

The author would like to thank Dr. Masaaki Kobayashi and Isao Hirohama of Mitsubishi Electric Corporation's Communication Systems Center and Takashi Iwamoto of Mitsubishi Electric Corporation's Advanced Technology R&D Center for numerous helpful discussions.

References

1) R. G. Wiley: Electronic intelligence: The analysis of radar signals (2nd ed.), Artech House, 237/249 (1993)
2) J. B. Moore and V. Krishnamurthy: Deinterleaving pulse trains using discrete-time stochastic dynamic-linear models, *IEEE Trans. Signal Processing*, **42**-11, 3092/3103 (1994)
3) A. Logothetis and V. Krishnamurthy: An interval-amplitude algorithm for deinterleaving stochastic pulse train sources, *IEEE Trans. Signal Processing*, **46**-5, 1344/1350 (1998)
4) B. M. Sadler and S. D. Casey: On periodic pulse interval analysis with outliers and missing observations, *IEEE Trans. Signal Processing*, **46**-11, 2990/3002 (1998)
5) T. Conroy and B. Moore: The limits of extended Kalman filtering for pulse train deinterleaving, *IEEE Trans. Signal Processing*, **46**-12, 3326/3332 (1998)
6) R. J. Orsi, J. B. Moore and R. E. Mahony: Spectrum estimation of interleaved pulse trains, *IEEE Trans. Signal Processing*, **47**-6, 1646/1653 (1999)
7) K. Nishiguchi: A new method for estimation of pulse repetition intervals, *National Convention Record of IEICE of Japan*, Information and Systems Section, 1-1 (1983) (in Japanese)
8) K. Nishiguchi and M. Kobayashi: Improved algorithm for estimating pulse repetition intervals, *IEEE Trans. Aerospace and Electronic Systems*, **36**-2, 407/421 (2000)
9) L. Schwartz: Théorie des distributions, Hermann, Paris 1966
10) C. K. Chui: An introduction to wavelets, Academic Press, 1992
11) C. K. Chui: Wavelets: A Mathematical Tool for Signal Analysis, SIAM, 1997
12) S. Moriguchi, K. Udagawa, and S. Hitotsumatsu: Mathematical Formulae, Vol. 3, Iwanami Shoten, 1987 (in Japanese)

Appendix A. Derivation of false alarm probability

To calculate the false alarm rate, the probability density function (pdf) of the noise of the PRI transform is needed. In general, a pdf is the Fourier transform of the corresponding characteristic function; hence, we may obtain the characteristic function. Since the PRI map is a complex-valued random variable, its pdf and also its characteristic function are two-dimensional functions. When there is one input in a PRI bin, the PRI map becomes

$$D_1 = e^{i\Theta}, \tag{A. 1}$$

where Θ is a random variable with uniform distribution on $[0, 2\pi]$. Let ξ, η be the parameters of the two-dimensional characteristic function of the PRI map. The characteristic function of D_1, which only depends on distance $s = \sqrt{\xi^2 + \eta^2}$ in ξ, η space, is calculated as

$$\begin{aligned}\phi_1(s) &= E\exp[i(\xi\cos\Theta + \eta\sin\Theta)] \\ &= \frac{1}{2\pi}\int_0^{2\pi}\exp[i(\xi\cos\theta + \eta\sin\theta)]d\theta \\ &= \frac{1}{2\pi}\int_0^{2\pi}\exp[is\cos\theta]d\theta = J_0(s),\end{aligned} \tag{A. 2}$$

where $J_0(\cdot)$ is the zeroth order Bessel function. When there are ℓ inputs in a PRI bin, the PRI map becomes

$$D_\ell = \sum_{j=1}^{\ell} e^{i\Theta_j}, \tag{A. 3}$$

whose characteristic function equals the ℓ-th power of that with one input, because $\Theta_j,\ j = 1, \cdots, \ell$ are independent of each other. Since the number of arrivals L to a PRI bin follows a Poisson distribution with parameter λ, the pdf becomes

$$p_\ell \equiv \mathcal{P}(L=\ell) = \frac{\lambda^\ell}{\ell!}e^{-\lambda}, \quad \ell = 0,1,2,\cdots, \qquad (A.4)$$

and both its mean and variance are equal to λ. From the above expression, the characteristic function of the noise component of the PRI map can be expressed in terms of distance variable s such that

$$\begin{aligned}\phi(s) &= \sum_{\ell=0}^{\infty} p_\ell J_0^\ell(s) = \sum_{\ell=0}^{\infty} \frac{\lambda^\ell}{\ell!}e^{-\lambda}J_0^\ell(s) \\ &= \exp[\lambda(J_0(s)-1)]. \end{aligned} \qquad (A.5)$$

Taking the 2-dimensional Fourier transform of $\phi(s)$, we obtain the 2-dimensional pdf of $D_{\rm N}$:

$$\begin{aligned}\hat{\phi}(r) &= \frac{1}{(2\pi)^2}\int_{-\infty}^{\infty}\int_{-\infty}^{\infty}\phi(s)e^{-i(x\xi+y\eta)}d\xi d\eta \\ &= \frac{1}{(2\pi)^2}\int_0^{\infty}\int_0^{2\pi}\phi(s)e^{-irs\cos\theta}sd\theta ds \\ &= \frac{1}{2\pi}\int_0^{\infty}s\phi(s)J_0(rs)ds, \end{aligned} \qquad (A.6)$$

from which the pdf of $|D_{\rm N}|$ is obtained as follows:

$$p(r) = 2\pi r\hat{\phi}(r) = \int_0^{\infty} rs\phi(s)J_0(rs)ds. \qquad (A.7)$$

The false alarm probability for threshold Γ is expressed as

$$P_{\rm FA}(\Gamma) \equiv \mathcal{P}(|D_{\rm N}| > \Gamma) = 1 - P(\Gamma), \qquad (A.8)$$

where $P(\,\cdot\,)$ is a cumulative distribution function (cdf). By calculating the cdf using (A. 7), we obtain

$$\begin{aligned}P(u) &= \mathcal{P}(|D_{\rm N}| \le u) = \int_0^u p(r)dr \\ &= \int_0^{\infty}\phi(s)\int_0^u rsJ_0(rs)drds \\ &= \int_0^{\infty}\phi(s)uJ_1(us)ds, \end{aligned} \qquad (A.9)$$

where $J_1(\cdot)$ is a first order Bessel function and the following relation is used:

$$\int_0^u rsJ_0(rs)dr = uJ_1(su). \qquad (A.10)$$

Substituting (A. 9) into (A. 8), we obtain the false alarm probability as follows:

$$P_{\rm FA}(\Gamma) = 1 - \Gamma\int_0^{\infty}\phi(s)J_1(\Gamma s)ds. \qquad (A.11)$$

Appendix B. Calculation of signal intensities

Without loss of generality, we assume $\nu \le w$; otherwise, we may replace ν by $\nu' = \min(\nu, w)$. First, we investigate the signal intensity when there is no mixing pulse, i.e., $q = 0$. In this case the PRI map at the PRI bin corresponding to τ is

$$D_0 = \sum_{n=1}^{\nu} e^{2\pi i t_n/\tau}. \qquad (B.1)$$

In general, let X be a random variable that is distributed uniformly in $[-\zeta/2, \zeta/2]$, and then it holds that

$$\begin{aligned}Ee^{2\pi iX} &= \int_{-\zeta/2}^{\zeta/2} e^{2\pi ix}\frac{1}{\zeta}dx = \left[\frac{1}{2\pi i\zeta}e^{2\pi ix}\right]_{-\zeta/2}^{\zeta/2} \\ &= \frac{e^{\pi i\zeta} - e^{-\pi i\zeta}}{2\pi i\zeta} = \frac{\sin(\pi\zeta)}{\pi\zeta} \equiv \mathrm{sinc}(\zeta). \end{aligned} \qquad (B.2)$$

Substituting (32) into (B. 1) and calculating the expectation of $|D_0|^2$ by (B. 2) yields

$$\begin{aligned}I_0^2 &\equiv E|D_0|^2 = E\sum_{n,m=1}^{\nu} e^{2\pi i(t_m - t_n)/\tau} \\ &= \sum_{n,m=1}^{\nu}\mathrm{sinc}^{|m-n|}(\zeta) \\ &= \nu\frac{1+\mathrm{sinc}(\zeta)}{1-\mathrm{sinc}(\zeta)} - \frac{2\mathrm{sinc}(\zeta)[1-\mathrm{sinc}^\nu(\zeta)]}{[1-\mathrm{sinc}(\zeta)]^2}. \end{aligned} \qquad (B.3)$$

Next, using the above result, we calculate the signal intensity when there are mixing pulses as follows:

$$\begin{aligned}I_{\rm S}^2 &\equiv E\left|\sum_{n=1}^{\nu}(1+U_n+V_n)e^{2\pi i t_n/\tau}\right|^2 + E|D'_{\rm N}|^2 \\ &= \sum_{m,n=1}^{\nu} E\left[(1+U_m+V_m)(1+U_n+V_n)\right. \\ &\qquad \left.\cdot\, e^{2\pi i(t_m-t_n)/\tau}\right] + q^2bw \\ &= \sum_{m,n=1}^{\nu} E(1+U_m+V_m)(1+U_n+V_n) \\ &\qquad \cdot Ee^{2\pi i(t_m-t_n)/\tau} + q^2bw, \end{aligned} \qquad (B.4)$$

whose first expectation is further calculated as

$$\begin{aligned}&E(1+U_m+V_m)(1+U_n+V_n) \\ &= (1+2bq)^2 + E(U_m-bq)(U_n-bq) \\ &\quad + E(V_m-bq)(V_n-bq) \\ &= \begin{cases}(1+2bq)^2+2bq, & n=m \\ (1+2bq)^2, & n\ne m\end{cases} \end{aligned} \qquad (B.5)$$

Substituting this into (B. 4) and using (B. 3), we obtain

$$\begin{aligned}I_{\rm S}^2 &= \sum_{n,m=1}^{\nu}\mathrm{sinc}^{|m-n|}(\zeta)(1+2bq)^2 + 2\nu bq + q^2bw \\ &= (1+2bq)^2I_0^2 + (qw+2\nu)bw. \end{aligned} \qquad (B.6)$$

Ken'ichi Nishiguchi (Member)

He received a B.S. degree in mathematics from Kyoto University in 1974 and a Ph.D. degree in engineering from Osaka University in 1994. In 1974 he joined Mitsubishi Electric Corporation's Central Research Laboratory (reorganized as the Advanced Technology R&D Center). Since 2007, he has been a specially appointed professor at Osaka University. His research interests include modeling and the analysis of stochastic systems, statistical signal and image processing, and nonlinear optics.

Reprinted from Trans. of the SICE
Vol. 40 No. 11 1114/1123 2004